Synchronization in area-preserving maps: Effects of mixed phase space and coherent structures

Sasibhusan Mahata,* Swetamber Das,† and Neelima Gupte‡
Department of Physics, Indian Institute of Technology Madras, Chennai 600036, India
(Received 13 June 2015; revised manuscript received 9 November 2015; published 10 June 2016)

The problem of synchronization of coupled Hamiltonian systems presents interesting features due to the mixed nature (regular and chaotic) of the phase space. We study these features by examining the synchronization of unidirectionally coupled area-preserving maps coupled by the Pecora-Caroll method. The master stability function approach is used to study the stability of the synchronous state and to identify the percentage of synchronizing initial conditions. The transient to synchronization shows intermittency with an associated power law. The mixed nature of the phase space of the studied map has notable effects on the synchronization times as is seen in the case of the standard map. Using finite-time Lyapunov exponent analysis, we show that the synchronization of the maps occurs in the neighborhood of invariant curves in the phase space. The phase differences of the coevolving trajectories show intermittency effects, due to the existence of stable periodic orbits contributing locally stable directions in the synchronizing neighborhoods. Furthermore, the value of the nonlinearity parameter, as well as the location of the initial conditions play an important role in the distribution of synchronization times. We examine drive response combinations which are chaotic-chaotic, chaotic-regular, regular-chaotic, and regular-regular. A range of scaling behavior is seen for these cases, including situations where the distributions show a power-law tail, indicating long synchronization times for at least some of the synchronizing trajectories. The introduction of coherent structures in the system changes the situation drastically. The distribution of synchronization times crosses over to exponential behavior, indicating shorter synchronization times, and the number of initial conditions which synchronize increases significantly, indicating an enhancement in the basin of synchronization. We discuss the implications of our results.

DOI: 10.1103/PhysRevE.93.062212

I. INTRODUCTION

Hamiltonian and area-preserving systems show a variety of intriguing features due to the mixed nature of their phase space. Some of the unique features seen in the case of Hamiltonian systems include the existence of anomalous kinetics, Lévy processes and Lévy flights [1], power-law contributions to recurrence and other statistics, and the existence of dynamical traps [2,3]. Phenomena like synchronization show different features in the case of Hamiltonian systems compared to those seen in the case of dissipative systems. In this paper we study the synchronization behavior of area-preserving maps, as models of Hamiltonian systems, where the maps are synchronized using the method of Pecora and Carroll [4]. The synchronization of dissipative systems using this method is well explored, both in theoretical and experimental contexts [5–12]. However, synchronization in Hamiltonian or area-preserving systems has not been explored in many studies. One example of this is Ref. [13], where Heagy and Carroll have demonstrated the existence of chaotic synchronization in Hamiltonian systems as represented by a standard map. They derive the synchronization conditions analytically and verify them numerically. They have also shown the phenomenon in an experimental realization of the "piecewise linear standard map" in an analog electric circuit. We note that two dynamical systems will be said to be completely *synchronized* if the difference between any of their quantifiable state properties converges to zero as $t \to \infty$.

Yet another form of coherent evolution is exhibited by a coupled Hamiltonian system wherein the two orbits share the same region of the individual phase space with identical invariant measures. This form of synchronization, known as measure synchronization, has been observed numerically in globally coupled standard maps [14], coupled ϕ^4 Hamiltonian systems [15], and Duffing Hamiltonians [16]. More generalized definitions of synchronization can be found in the numerous reviews on the subject [17–19]. In the present work, synchronization is considered in the strict sense of complete synchronization alone, and phenomena like generalized synchronization and measure synchronization will be dealt with elsewhere.

In the context of the present paper, we examine the synchronization behavior seen on the synchronization properties of Hamiltonian systems, as represented by area-preserving maps. We use the standard map [20], the prototypical area-preserving map, as our example. Here, a pair of standard maps are coupled unidirectionally using Pecora-Caroll coupling. This system was first examined by Heagy and Caroll [13]. They obtained the synchronization criterion for this system in terms of the conditional Lyapunov exponent (also known as the master stability function) and said that the system should show synchronizing trajectories when the average conditional Lyapunov exponent was negative. However, Heagy and Caroll observed that synchronizing trajectories were seen for the system considered for values of the nonlinearity parameter which greatly exceeded the value of nonlinearity at which the conditional Lyapunov exponent was positive. Heagy and Caroll correctly attributed this phenomenon to the nonuniformity of the measure in phase space, i.e., to the effect of the mixed nature of the phase space, which contains regular regions, chaotic trajectories, and sticky

*sasibhusan@physics.iitm.ac.in
†swetdas@physics.iitm.ac.in
‡gupte@physics.iitm.ac.in

regions, but did not explore the consequences of this mixed nature.

In this paper, we examine in detail the effects of the mixed phase space on a variety of quantities of interest for the synchronization problem. The effect of the nature of initial conditions on the master stability functions, and on synchronization properties such as distributions of synchronization times, are explored. Here, we see intermittent synchronization in the transient until synchronization is achieved. The laminar lengths in this distribution obey power-law behavior. We find that synchronization occurs in the neighborhood of the invariant curves in the phase space. We confirm this via finite-time analysis of the conditional Lyapunov exponent in the angular direction of the coupled standard map considered. The existence of such trapping or sticky regions in the phase space of area-preserving systems has been noted earlier [2,3] and is known to have important implications for transport [21]. We also identify the presence of stable periodic orbits in the vicinity of these sticky neighborhoods. The presence of stable periodic trajectories in these neighborhoods provides local transverse stable directions, so trajectories which enter these neighborhoods tend to converge in the time which they spend in these neighborhoods, giving rise to laminar regions in the time series of the separation between trajectories and are interspersed by chaotic bursts which are seen when the trajectories leave these neighborhoods. Similar effects are seen due to unstable periodic trajectories in the studies of Heagy, Pecora, and Carroll [22], but the effect is reversed, as the unstable directions push away trajectories which are synchronizing, leading to the chaotic burst intervals in the intermittent time series.

We also find that the distribution of synchronization times has a power-law tail, for all combinations of initial conditions (those which lead to regular or chaotic trajectories). Synchronization can be seen even at parameter values where the average Lyapunov exponents computed from the master stability function are positive, this being due to the existence of a finite fraction of synchronizing initial conditions, even at these parameter values. The introduction of a coherent structure in the phase space leads to a huge reduction in synchronization times, and a corresponding exponential distribution for the synchronization times, as well as a substantial increase in the number of initial conditions which synchronize. The introduction of a coherent structure is thus an effective strategy to enhance synchronization and reduce synchronization times.

This paper is organized as follows. In Sec. II, we describe the simple unidirectional coupling scheme used to couple the area-preserving maps under investigation and compute the Lyapunov exponents from the master stability function for the coupled system. Synchronization in the coupled standard map is demonstrated and analyzed in Sec. III. Section IV studies the distributions of synchronization times and the effect of initial conditions in detail. This section also examines the distributions of finite-time Lyapunov exponents and the role of periodic orbits. In Sec. V, we introduce a coherent structure in the coupled systems and study its effect of synchronization and synchronization times. Our results and their implications are discussed in Sec. VI.

II. THE COUPLED STANDARD MAP

The standard map is considered to be the prototypical example of a two-dimensional area-preserving map and is given by:

$$\left.\begin{aligned} P_{n+1} &= P_n + K \sin Q_n \\ Q_{n+1} &= P_{n+1} + Q_n \end{aligned}\right\} \bmod 2\pi. \tag{1}$$

Here, the subscript n denotes the discrete time and K is the nonlinearity parameter. These equations typically describe the evolution of two canonical variables P and Q which correspond to the momentum and coordinate in the Poincaré section of a kicked rotator, a system which represents the behavior of a variety of mechanical systems, as well as the behavior of accelerator systems. Two-dimensional phase space plots of the standard map for the parameter values $K = 1.5$ and $K = 6$ using 25 initial conditions are shown in Figs. 1(a) and 1(b).

We now synchronize two standard maps, using the Pecora-Carroll scheme of synchronization using drive-response coupling [4]. This system was first devised to synchronize dissipative chaotic dynamical systems, and first demonstrated

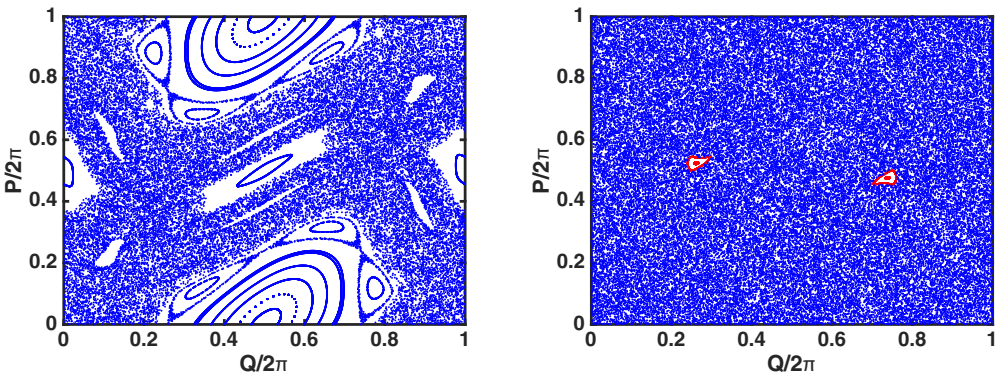

(a) (b)

FIG. 1. The phase space of the standard map for 25 random initial conditions from the uniform distribution on $[0,2\pi]$ plotted for 4500 iterations; 500 iterates are discarded as transients. The values are normalized, i.e., $\frac{P}{2\pi}$ and $\frac{Q}{2\pi}$ are plotted on the y and x axes for the parameter values (a) $K = 1.5$ and (b) $K = 6.0$. Most of the phase space is covered by chaotic trajectories. However, small coherent structures can be seen at the edge, and in the middle of the white regions.

that even chaotic trajectories can be effectively synchronized. Under this unidirectional coupling scheme, we duplicate the given map and couple the original and the duplicated map in a drive-response configuration. This means that the drive map evolves freely but the evolution of the response map is dependent on the drive. In this case, the P value of the response system is set to the P value of the drive system at each iterate. Therefore, the coupled system is described by the following equations:

$$\left.\begin{aligned} P^d_{n+1} &= P^d_n + K\sin Q^d_n \\ Q^d_{n+1} &= P^d_{n+1} + Q^d_n \end{aligned}\right\} \bmod 2\pi \text{ (Drive)}, \tag{2}$$

$$\left.\begin{aligned} P^r_{n+1} &= P^d_n + K\sin Q^r_n \\ Q^r_{n+1} &= P^r_{n+1} + Q^r_n \end{aligned}\right\} \bmod 2\pi \text{ (Response)}. \tag{3}$$

The initial values of Q in the drive and response maps are chosen arbitrarily, whereas the P values are identical. The system is said to reach complete synchronization when both the P and Q values of the drive and response systems evolve to identical values. We analyze the synchronization of this system using the master stability function [23].

Master stability function

A general drive-response system coupled unidirectionally may be described by the following set of equations:

$$\frac{d\overline{X}_d}{dt} = \overline{F}(\overline{X}_d), \quad \frac{d\overline{X_r}}{dt} = \overline{F}(\overline{X}_r) + \alpha E(\overline{X}_d - \overline{X}_r).$$

Here $\overline{X}_d$ and $\overline{X}_r$ are drive and response variables; the matrix E determines the linear combination of the $\overline{X}$ used in the difference and α is the coupling strength. For the map case, we have the following form

$$\overline{X}^d_{n+1} = \overline{F}\left(\overline{X}^d_n\right), \quad \overline{X}^r_{n+1} = \overline{F}\left(\overline{X}^r_n\right) + \alpha E\left(\overline{X}^d_n - \overline{X}^r_n\right).$$

Therefore, in the case of a general unidirectional coupling of two standard maps, we get

$$\left.\begin{aligned} P^d_{n+1} &= P^d_n + K\sin Q^d_n \\ Q^d_{n+1} &= P^d_{n+1} + Q^d_n \\ P^r_{n+1} &= P^r_n + K\sin Q^r_n + \alpha\left(P^d_n - P^r_n\right) \\ Q^r_{n+1} &= P^r_{n+1} + Q^r_n \end{aligned}\right\} \bmod 2\pi. \tag{4}$$

We have chosen E to be the matrix $\left[\begin{smallmatrix}1 & 0\\ 1 & 0\end{smallmatrix}\right]$.

To find the stability of the synchronous state, we first express Eq. (4) in terms of $P^\perp = P^d - P^r$ and $Q^\perp = Q^d - Q^r$ as follows:

$$\begin{aligned} P^\perp_{n+1} &= (1-\alpha)P^\perp_n + K\sin\left(Q^d_n\right) - K\sin\left(Q^r_n\right) \\ Q^\perp_{n+1} &= (1-\alpha)P^\perp_n + Q^\perp_n + K\sin\left(Q^d_n\right) - K\sin\left(Q^r_n\right). \end{aligned} \tag{5}$$

We now write the variational equation for Eq. (5) by linearizing about (P^d_n, Q^d_n)

$$\begin{bmatrix}\delta P^\perp_{n+1}\\ \delta Q^\perp_{n+1}\end{bmatrix} = \mathcal{M}\begin{bmatrix}\delta P^\perp_n\\ \delta Q^\perp_n\end{bmatrix}, \tag{6}$$

where the matrix $\mathcal{M}$ is given by

$$\mathcal{M} = \begin{bmatrix}1-\alpha & K\cos\left(Q^d_n\right)\\ 1-\alpha & 1+K\cos\left(Q^d_n\right)\end{bmatrix}, \tag{7}$$

which is the Jacobian matrix for the variational equation (6), the master stability equation for the coupled system under investigation. The associated largest Lyapunov exponent (LE) computed from the master stability equation is the master stability function (MSF) of the system as follows. The Jacobian matrix for n-times iterated map is given by

$$\mathcal{M}^n = \mathcal{M}(\overline{X}_{n-1}).\mathcal{M}(\overline{X}_{n-2})\cdots\mathcal{M}(\overline{X}_0). \tag{8}$$

If Λ^k_i denotes the kth eigenvalue of the matrix $\mathcal{M}^n$ at the ith iteration of the map, then the Lyapunov exponents (LE-s) are given by

$$\lambda^k = \lim_{n\to\infty}\frac{1}{n}\sum_{i=0}^{n-1}\ln\left|\Lambda^k_i(n)\right|. \tag{9}$$

A negative value of the MSF (the largest nonzero LE) will ensure that $(P^\perp, Q^\perp)$ tends to zero, indicating that the difference between P and Q will die out and the system will synchronize. An analytic criterion for generalized synchronization using a different approach has been derived in Ref. [24].

Now, for the Pecora-Carroll approach, we set $\alpha = 1$. This substitution simplifies the matrix in Eq. (7), which now reads

$$\mathcal{M}_1 = \begin{bmatrix}0 & K\cos\left(Q^d_n\right)\\ 0 & 1+K\cos\left(Q^d_n\right)\end{bmatrix}. \tag{10}$$

The MSF should then be computed from the eigenvalues of the matrix $\mathcal{M}_1$. It is easy to see that, for $\alpha = 1$, one of the eigenvalues of $\mathcal{M}_1$, Λ_1, is zero. Therefore, we need to consider only the nonzero eigenvalue which is $\Lambda_2 = 1 + K\cos(Q^d_n)$. The corresponding LE is given by

$$\lambda = \lim_{n\to\infty}\frac{1}{n}\sum_{i=0}^{n-1}\ln\left|1+K\cos\left(Q^d_n\right)\right|. \tag{11}$$

The superscript k has been dropped as we have only one eigenvalue to compute. The variation of the LE λ is shown in Fig. 2(a) wherein λ is calculated and averaged over 50 000 randomly chosen initial conditions for different values of K. We note that the LE is negative up to $K = 2$, and crosses to positive values thereafter. However, due to the mixed nature of the phase space, synchronization can occur even for the values of K where the average LE is not negative. The plot in Fig. 2(a) also shows the LE exponents for synchronizing initial conditions and nonsynchronizing initial conditions separately. We plot the percentage of initial conditions which evolve to the synchronized state in Fig. 2(b). Trajectories that have not synchronized after 5000 iterations are counted as nonsynchronized. The nature of the distribution of synchronization times remains unchanged up to 10 000 iterations. It is clear that the LE is negative for synchronizing initial conditions and positive for nonsynchronizing ones, as it should be.

We find that more than 80% of the initial conditions synchronize for $K \leqslant 3$ but, for higher values of K, the synchronizing fraction drops to almost 1% of the whole. We

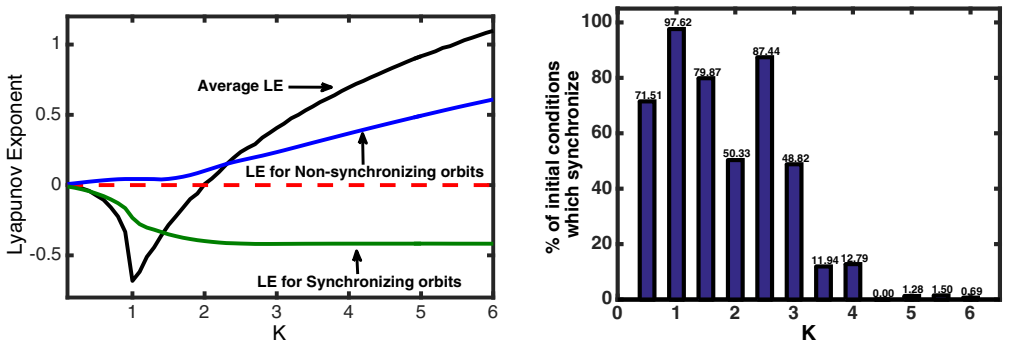

(a) (b)

FIG. 2. (a) The variation of the Lyapunov exponent as a function of K. The LEs have been calculated and averaged over 5000 initial conditions randomly chosen from the interval $[0,2\pi]$ for 50 000 iterations in each case. It is seen that the LE values cross the zero line at $K = 2$ and remain positive afterwards. The three curves show the variation of LEs with K for synchronizing and nonsynchronizing orbits. (b) The percentage of the initial conditions that converge to synchronization for $K = (0.5, 1, 1.5, \ldots, 6)$. We have chosen 5000 initial conditions randomly chosen over the interval $[0,2\pi]$. The percentages are mentioned at the top of the bars. The synchronization accuracy used is 10^{-5}.

also note that a sizable fraction of initial conditions lead to synchronization at $K = 2.5$ and $K = 3$ where the average value of the LE is positive [compare with Fig. 2(b)]. This happens due to the fact that the LEs for nonsynchronizing orbits having non-negative values are larger in magnitude, and are also weighted by the fraction of nonsynchronizing initial conditions, which contributes to the increase in the average. Therefore, we obtain synchronization for some initial conditions even if the *average* LE is non-negative. In addition, we do not find any synchronization at $K = 4.5$, consistent with the corresponding LE. It is clear that synchronization in this system shows a strong dependence on the initial conditions. In the next section, we investigate whether the synchronization times also show this initial condition dependence.

III. SYNCHRONIZATION: THE BEHAVIOR OF THE TRANSIENT AND INTERMITTENCY

Complete synchronization between the drive and response maps in the case of the coupled standard map is said to be achieved if $\Delta Q(=Q_n^d - Q_n^r) = 0$. Such a case is shown in Fig. 3 for $K = 1.5$ for one set of initial conditions (drive, response). Here, two trajectories are said to be synchronized to numerical accuracy if the Euclidean distance between them is less than $\delta = 10^{-5}$.

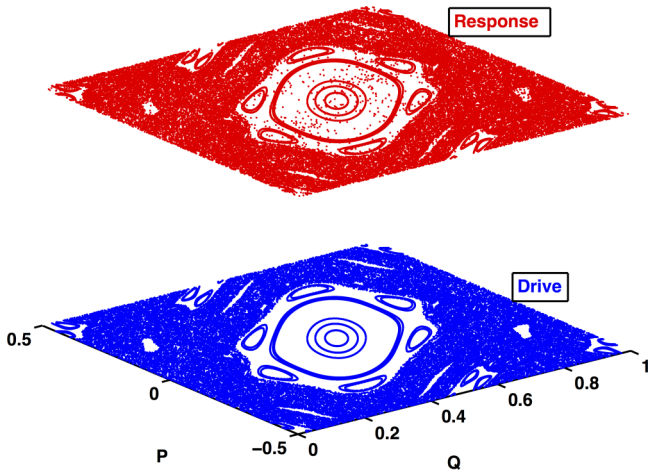

FIG. 3. The synchronized drive and response systems of two standard maps coupled via the "Pecora-Carroll coupling" scheme at $K = 1.5$ after a transient of 500 iterates.

It is interesting to ask whether there are regions in the phase space where the trajectories have a greater tendency to synchronize; i.e., Are there regions which function as synchronization "traps"? In order to identify such regions, we follow drive and response pairs of initial conditions via their trajectories to the points where they get locked onto each other and identify the location of such points in phase space.

If we follow the individual trajectories of the drive and response maps in the phase space, then we find that the points at which both the maps synchronize, i.e., the Q values of the drive and the response maps become identical within numerical accuracy, either lie on one of the invariant curves or appear to be in the close neighborhood of the invariant curves. The location of the synchronization points lies on, or in the neighborhood of, the invariant curves, irrespective of whether the initial conditions chosen for a drive or response system lie in the regular or the chaotic region of the mixed phase space of the map. Figure 4 demonstrates an example.

In Fig. 4, the evolution of the iterates of the drive and response maps near synchronization is shown on the left [Figs. 4(a), 4(c), 4(e), and 4(g)] and the corresponding variation in ΔQ is shown on the right [in Figs. 4(b), 4(d), 4(f), and 4(h)]. The initial conditions for the drive and response maps have been chosen from the chaotic region and are indicated by the solid left triangle "◁" (in blue) and the solid right triangle "▷" (in red), respectively, in the plots on the left. The iterates belonging to the drive map (shown by the symbol "◁" in blue) appear to be distributed randomly in Fig. 4(a) as these are a part of a chaotic trajectory due to the choice of initial conditions. The response maps iterates (shown by the symbol "▷" in red) are determined by the drive in Eq. (2) and the difference between the drive and response, viz. ΔQ, fluctuates continuously as in Fig. 4(b). The drive iterates then appear to approach an invariant curve in the phase space followed by the response, and the difference ΔQ begins to approach zero [Figs. 4(c) and 4(d)]. The locations of the drive and response iterates right before synchronization are shown in

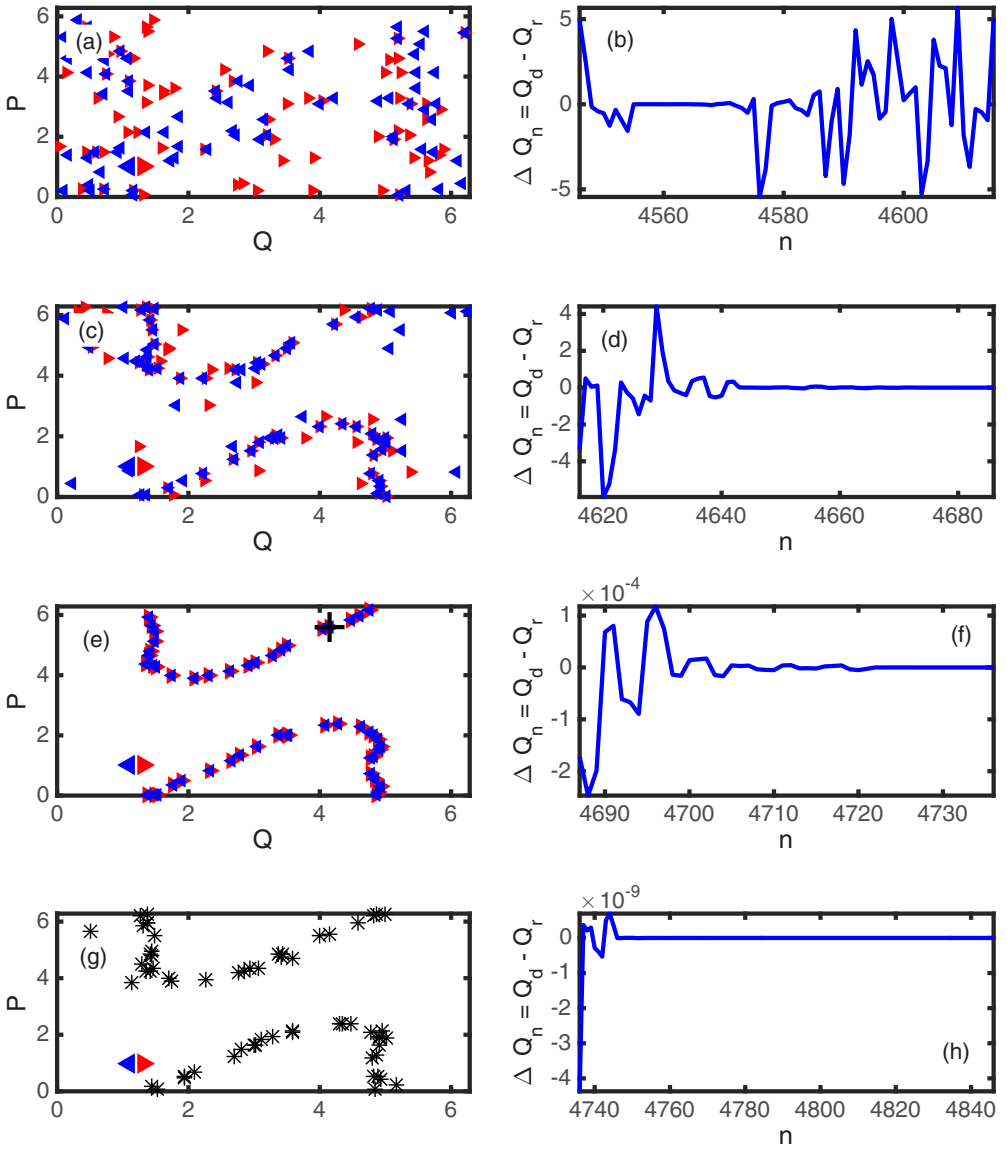

FIG. 4. The figure shows a typical trajectory of the drive and the response map for an initial condition chosen from the chaotic regime at $K = 1.5$. The iterates for the drive map are plotted using the left hollow triangle, "◁" in blue, and for the response map using the right hollow triangle, "▷" in red, in plots on the left of the panel. The synchronized iterates are shown by the asterisk "∗" in black. Complete synchronization is taken to be achieved if the iterates fall within a distance 10^{-5}. For more details, see the text in Sec. III.

Fig. 4(e). Note that the location indicated by the plus sign (+) is the point of synchronization. The fluctuation in ΔQ is now an order of magnitude less than 10^{-4} [Fig. 4(f)]. At the point of synchronization the response iterates lock onto those of the drive and the synchronized trajectory (which is the drive trajectory) evolves thereafter with ΔQ values which are almost zero [Figs. 4(g) and 4(h), respectively]. Thus, complete synchronization is achieved in the neighborhood of an invariant curve for a drive which is chaotic.

Figure 4 has been plotted for the initial condition $(Q_d, Q_r, P)_0 = (1.3, 1.1, 1)$. Synchronization occurs at $\tau = 4736$ at the (P, Q) values indicated in Fig. 4(e) by the "+" sign, in black. The phase-space plots [Figs. 4(a), 4(c), 4(e), and 4(g)] show, respectively, the location of 72 iterates (from $\tau - 190$ to $\tau - 121$), 71 iterates (from $\tau - 120$ to $\tau - 50$), 50 iterates ($\tau - 49$ to τ), and 61 iterates ($\tau + 50$ to $\tau + 110$). The corresponding variations in ΔQ_n are shown in Figs. 4(b), 4(d), 4(f), and 4(h).

We further observe that the transient to synchronization is seen to exhibit intermittent behavior in the quantity ΔQ [Fig. 5(a)] or, equivalently, the phase difference of the two maps in the transient. We find that the distribution of laminar regions in Fig. 5(a) scales as a power law for the values in the figure caption. The exponent is given by 0.9486 ± 0.013 for the log-log plot of the reverse cumulative distribution of laminar lengths in the given range. To explain the intermittent behavior of $(Q_d - Q_r)$, we note that both the trajectories together pass near invariant curves several times before actually collapsing on to each other giving rise to laminar and burst regimes. Thus, the laminar regimes indicate the time intervals during which the drive and the response trajectories remain close to one of the invariant curves.

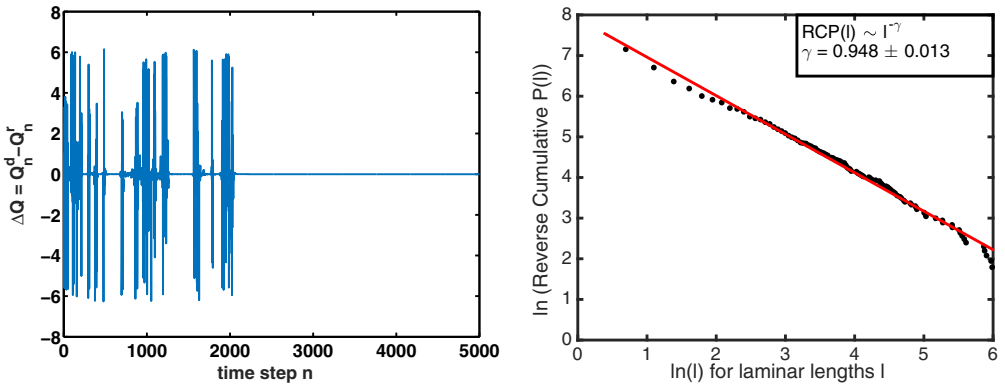

(a) (b)

FIG. 5. (a) Intermittent behavior in the quantity $\Delta Q = Q_n^d - Q_n^r$ in the coupled standard map leading to identical synchronization at $K = 1.5$ for 5000 iterations. (b) The log-log plot of the reverse cumulative distribution of the laminar lengths in the intermittent region at $K = 1.5$ shows power-law scaling with an exponent given by 0.9486 ± 0.013 for 50 000 randomly chosen initial conditions from the uniform distribution on the interval $[0, 2\pi]$ for the relevant variables.

These observations suggest that once drive and response trajectories evolve to the neighborhood of an invariant curve, they coalesce onto each other, leading to the synchronization of both trajectories. This is true for drive trajectories which are chaotic as well as those which lie on invariant curves. If the drive trajectory lies on an invariant curve, then the response trajectory collapses onto it very quickly and synchronization times are short. We discuss this in greater detail in the next section.

A. Finite-time Lyapunov exponent for the synchronizing subsystem

Dynamical traps in chaotic orbits are known to exist in an area-preserving map due to the stickiness of trajectories to some specific domains in phase space such as regular islands in the phase spaces of the web map and the standard map [2,3,25–27]. This means that close to those domains, the trajectories can spend an arbitrary long but finite time. In such trapping regions in the phase space, parts of a *chaotic* trajectory are almost regular. It has been shown that such traps in the web map and the standard map can be characterized using the properties of the finite-time Lyapunov exponent—the distribution of exponents is bimodal due to orbits sticking near elliptic regions [27]. In our numerical simulations, we find that the regular regions behave as traps for both drive and response trajectories. We can therefore apply a similar finite time Lyapunov exponent (FTLE) analysis to characterize those traps.

Following Sec. II A, we define the largest nonzero time-n Lyapunov exponent (FTLE λ_s) associated with an initial point $\overline{X}_0 = (P_0, Q_0)$ as

$$\lambda_s(\overline{X}_0; n) = \frac{1}{n} \sum_{i=0}^{n-1} \ln |\Lambda_i(n)|. \tag{12}$$

We extend this notion to the master stability function, i.e., the nonzero Lyapunov exponent defined in Eq. (11), given by $\Lambda_2 = 1 + K \cos(Q_n^d)$. The finite-time version of this is

$$\lambda_s(\overline{X}_0; n) = \frac{1}{n} \sum_{i=0}^{n-1} \ln |1 + K \cos Q_i|. \tag{13}$$

Next, we define the probability density of the FTLE $f(\lambda_s(\overline{X}_0; n))$ for a randomly chosen initial condition $\overline{X}_0 = (P_0, Q_0)$ which leads to chaotic orbit. This means that $f(\lambda_s(\overline{X}_0; n))d\lambda_s$ is the probability that the FTLE value lies between λ_s and $\lambda_s + d\lambda_s$. If $F(\lambda_s(n); n)$ is any function of the FTLE, then its average over the invariant chaotic measure is given by

$$\overline{F[\lambda_s(n)]} = \frac{\int_{-\infty}^{+\infty} F(\lambda_s(n) f(\lambda_s(n); n) d\lambda_s}{\int_{-\infty}^{+\infty} f(\lambda_s(n); n) d\lambda_s}. \tag{14}$$

We obtain the distribution $f(\lambda_s(n))$ numerically by choosing 1000 initial conditions distributed randomly over the phase-space regions covered by the chaotic sea and iterate them for 10 000 times to compute the FTLE at every $n = 8$ step for $K = 1.5$. The distribution thus found is shown in Fig. 6. The distribution is clearly bimodal. The large negative values indicate the synchronized state of the subsystem which

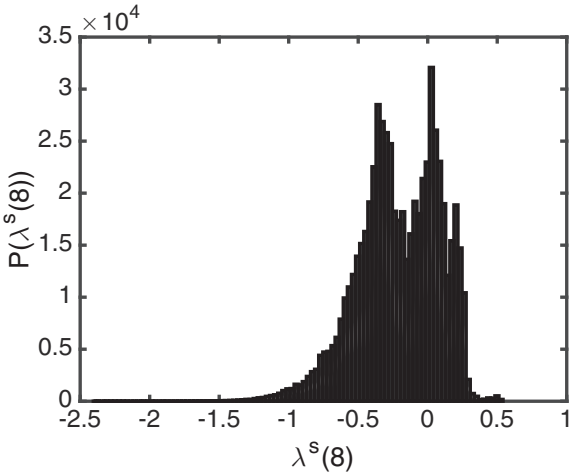

FIG. 6. The bimodal distribution of subsystem FTLEs, at $K = 1.5$, for 1000 randomly chosen initial conditions distributed uniformly over chaotic regions of the phase space. The number of iterations in each case is 10 000 and the average is computed for $n = 8$.

TABLE I. The table gives values of the Lyapunov exponents (in the second row) computed for the periodic orbits (first row) at $K = 1.5$ using the Newton-Raphson search algorithm. Negative values indicate the local stability of the synchronization manifold for the orbits.

Orbit	13	25	30	35	40	44	50	60	70
λ_f	−0.1273	−0.0277	−0.0234	−0.0203	−0.0198	−0.0159	−0.0148	−0.0268	−0.0999

occurs in the sticky regions in the neighborhood of invariant curves. The comparatively small positive values close to zero correspond to the initial expanding directions of the trajectories. This is similar to the bimodal distribution found in Ref. [27] for the standard map at $K = 1.5$ in which small negative values of FTLE are due to the sticky regions and large positive values exist for those parts of the trajectories that lie in the chaotic bulk. Therefore, the FTLE analysis for the subsystem indicates that synchronization occurs in one of the sticky regions which traps the chaotic trajectories of the drive and the response maps. There is a close connection between the sticky regions and the periodic orbits of the system. We discuss this in the next section.

B. Role of periodic orbits

We note that the behavior of the synchronization traps can be analyzed in a more quantitative way by analyzing the location and stability properties of the periodic orbits in the vicinity of the locations where synchronization takes place. We compute the Lyapunov exponents of the periodic orbits themselves. First, a periodic orbit of the standard map is located by using a Newton-Raphson search algorithm [28]. There are infinitely many periodic orbits present in the regular regions of the phase space of the standard map. An initial guess here will lead to one of these periodic orbits. Next, the Floquet matrix is constructed for the variational Eq. (6) on the orbit that is located [28]. The Floquet matrix, F, relates an arbitrary initial variation about the periodic orbit, say, $\delta(0)$, to its value $\delta(T)$ after a complete period T, by the relation

$$\delta(T) = F\delta(0). \tag{15}$$

The eigenvalues of F are then the "Floquet multipliers" (α_1,α_2), for the located periodic orbit. Note that, for the case at hand, one of the multipliers, say, α_2, will always be zero, indicting no change in the P direction. The other exponent will then give the Lyapunov exponent for the periodic orbit

$$\lambda_f = \frac{\ln|\alpha_1|}{T}, \tag{16}$$

where T is the period of the orbit.

We have computed the Lyapunov exponent λ_f for several periodic orbits located using the Newton-Raphson method at $K = 1.5$. The exponent comes out to be negative in all the cases, indicating the local stability of the transverse synchronization manifold of the periodic orbits. Some of the computed values are listed in Table I.

It is also useful to identify the location of periodic orbits in the phase space. A periodic orbit of period 44 located using a Newton-Raphson search is shown in Fig. 7 for $K = 1.5$. The orbit is plotted on Fig. 4(e) to show its proximity with the location of the point of synchronization of the trajectories of Fig. 4 indicated by the cross in the figure.

Our analysis is similar to that of Ref. [22] wherein the synchronous chaotic behavior in coupled Rőssler-like oscillators, interrupted by bursts of desynchronized behavior, was analyzed by investigating the role of unstable periodic orbits during bursting events. It was found that periodic orbits within a synchronous chaotic attractor are locally unstable, thereby giving rise to intermittent burst regimes. In our case, the reverse behavior is seen as the periodic orbits are locally stable. The existence of these local stable directions accounts for the observed laminar regimes ΔQ before the eventual trapping of the chaotic trajectories of the drive and response maps and the final synchronization of the maps. As expected, the point at which the chaotic trajectories synchronize lies in the vicinity of the periodic trajectories.

IV. THE DISTRIBUTION OF SYNCHRONIZATION TIMES

Since the phase space of the standard map is mixed, a given initial condition may lead to a chaotic or a regular trajectory. We group our (drive, response) initial conditions according to the nature of the trajectory, which would have been obtained had the initial condition been allowed to evolve freely. Thus, the four possibilities for pairs of initial conditions for the (drive, response) system are as follows: (chaotic, chaotic), (chaotic, regular), (regular, regular), and (regular, chaotic). For the simulations reported herein, the accuracy in computation is 10^{-5}. Figure 8 shows the distribution of synchronization times and the location of initial conditions for each type of drive-response pair at $K = 1.5$ [Fig. 9 shows the pairs in a smaller region of Fig. 8(f)] and Fig. 10 shows those at $K = 6$. We have considered 10 000 initial conditions for $K = 1.5$ and 50 000 initial conditions for $K = 6$ chosen randomly from

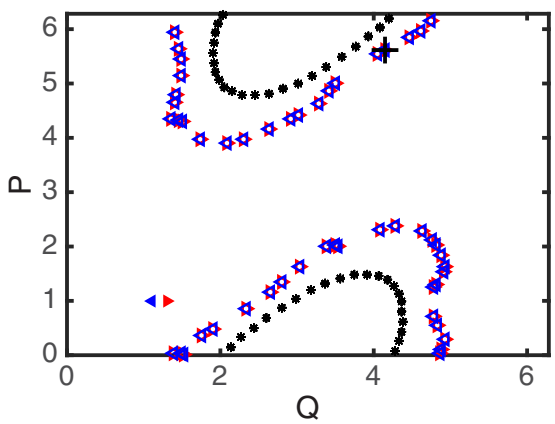

FIG. 7. This plot shows Fig. 4(e) with a periodic orbit with period 44 indicated by the black "∗." The Lyapunov exponent of the synchronization manifold for this periodic orbit at $K = 1.5$ is found to be −0.0159.

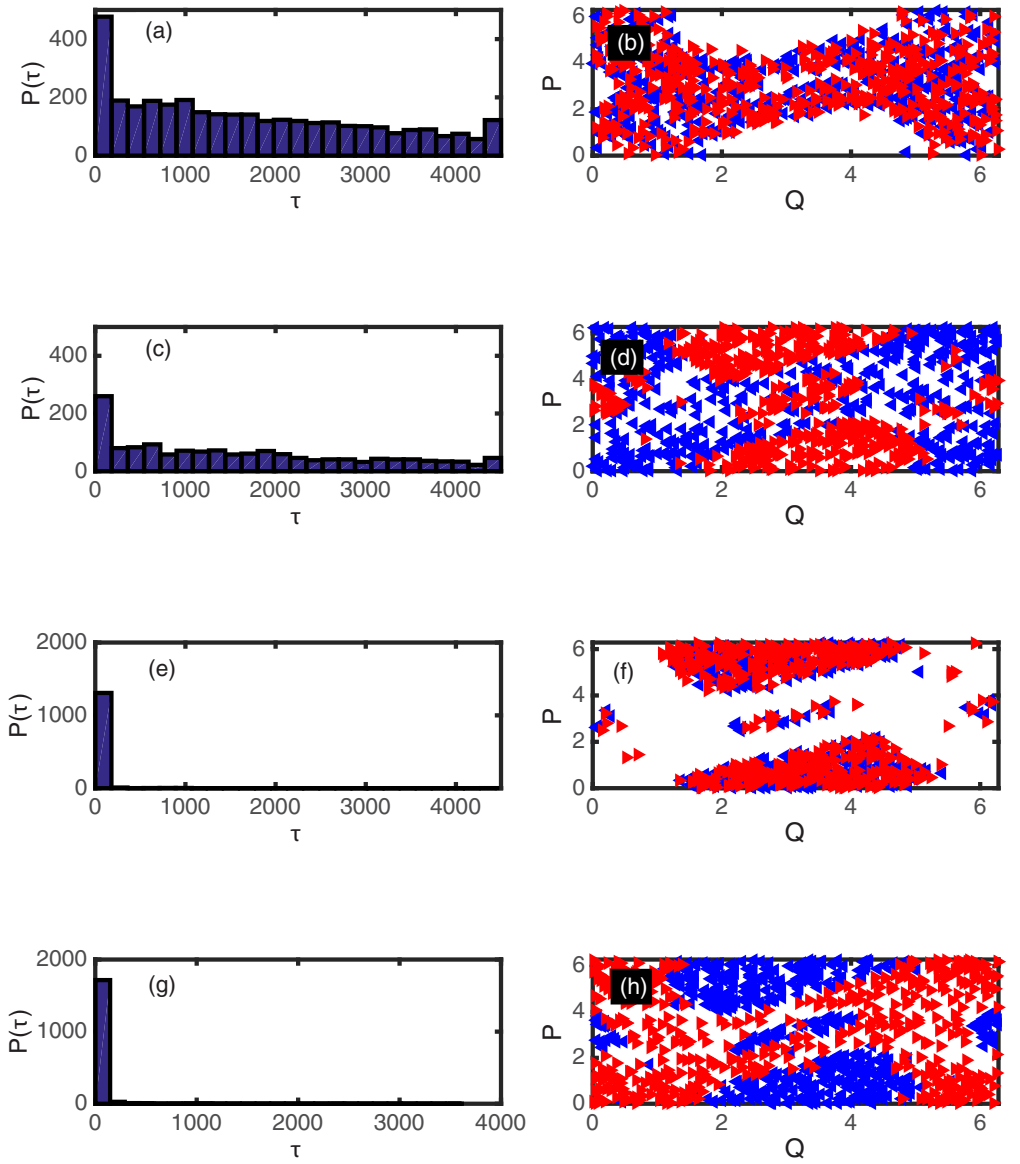

FIG. 8. The distribution of synchronization times and the location of initial conditions for the coupled standard map at K = 1.5 for (drive, response) maps in the [(a) and (b)] (chaotic, chaotic), [(c) and (d)] (chaotic, regular), [(e) and (f)] (regular, regular), and [(g) and (h)] (regular, chaotic) regimes. The initial conditions for the drive map are plotted using the left hollow triangle, "◁" in blue, and for the response map using the right hollow triangle, "▷" in red. Complete synchronization is taken to be achieved if the iterates fall within a distance 10^{-5}. For more details, see the text in the Sec. III. The distributions plotted on the left of the panel have 25 bins each for synchronization times for 10 000 different initial conditions randomly chosen for the uniform distribution on the interval $[0,2\pi]$. The locations of initial conditions in the plots on the right of the panel indicate the regions from which these initial conditions are chosen.

the uniform distribution $[0,2\pi]$. We did not find any (chaotic, regular) pair which synchronizes at $K = 6$.

It is observed that with the increase of the nonlinearity parameter K, the number of initial conditions that show synchronization decreases. For instance, at $K = 6$, only about 0.7% of the chosen initial conditions lead to synchronized behavior. The synchronization time distribution for all the pairs collectively shows a very long tail as in Fig. 11(a) for 50 000 different initial conditions randomly chosen from the uniform distribution on the interval [0,1]. Interestingly, the tail in the distribution shows power-law scaling [Fig. 11(b)] with the exponent of the cumulative distribution being given by 1.117 ± 0.030. In Table II, we have estimated the exponent for the categories (chaotic, chaotic) and (chaotic, regular) at $K = (1.5, 4.0, 6.0)$ for 5000 and 10 000 iterations for randomly chosen initial conditions in the interval $[0,2\pi]$. The tail of the distribution corresponds to long synchronization times, and the power-law decay indicates that in addition to the fact that a very small number of initial conditions synchronize here, a significant fraction of these exhibit a very slow rate of convergence.

We note that the phase-space structure seen here is fairly homogeneous at this high value of the nonlinearity parameter K, with most of the phase space being accessed by chaotic trajectories, and the exponents settle down into more stable values. On the other hand, for lower values of K, the phase

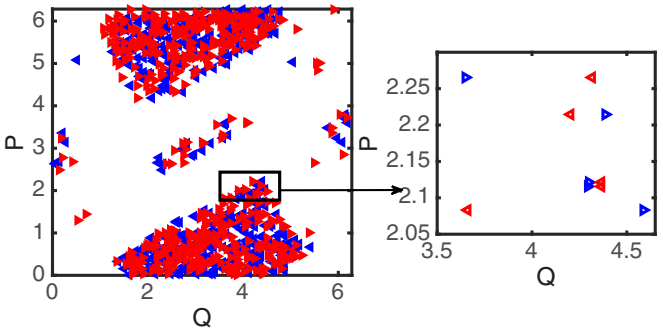

FIG. 9. A part of Fig. 8(f) is blown up to show that the "P" are taken to be identical for the drive [indicated by the plus sign (+) in blue] and response maps (indicated by "∗" in red).

space is inhomogeneous, as many periodic orbits exist in the space. This leads to a greater dependence of the power-law exponent on the number of iterates. It is interesting to see whether the introduction of a large inhomogeneity in the phase space can contribute to an increase in the basin of synchronization and to a reduction in the synchronization times. A large inhomogeneity in the phase space can be introduced by creating a coherent structure in the system. We also find that the introduction of a coherent structure in the system has a remarkable effect on the synchronization times, as described in the next section.

V. THE EFFECT OF A COHERENT STRUCTURE ON SYNCHRONIZATION

Many of the effects seen in the synchronization behavior of the standard map are due to the mixed nature of the phase space. It is therefore interesting to see whether the existence of a coherent structure has a significant effect on the synchronization behavior of the standard map. Coherent structures are regular and localized structures in the phase space of chaotic and turbulent dynamical systems. These structures are stable and not affected by the chaotic nature of the system. A coherent structure can be generated in the

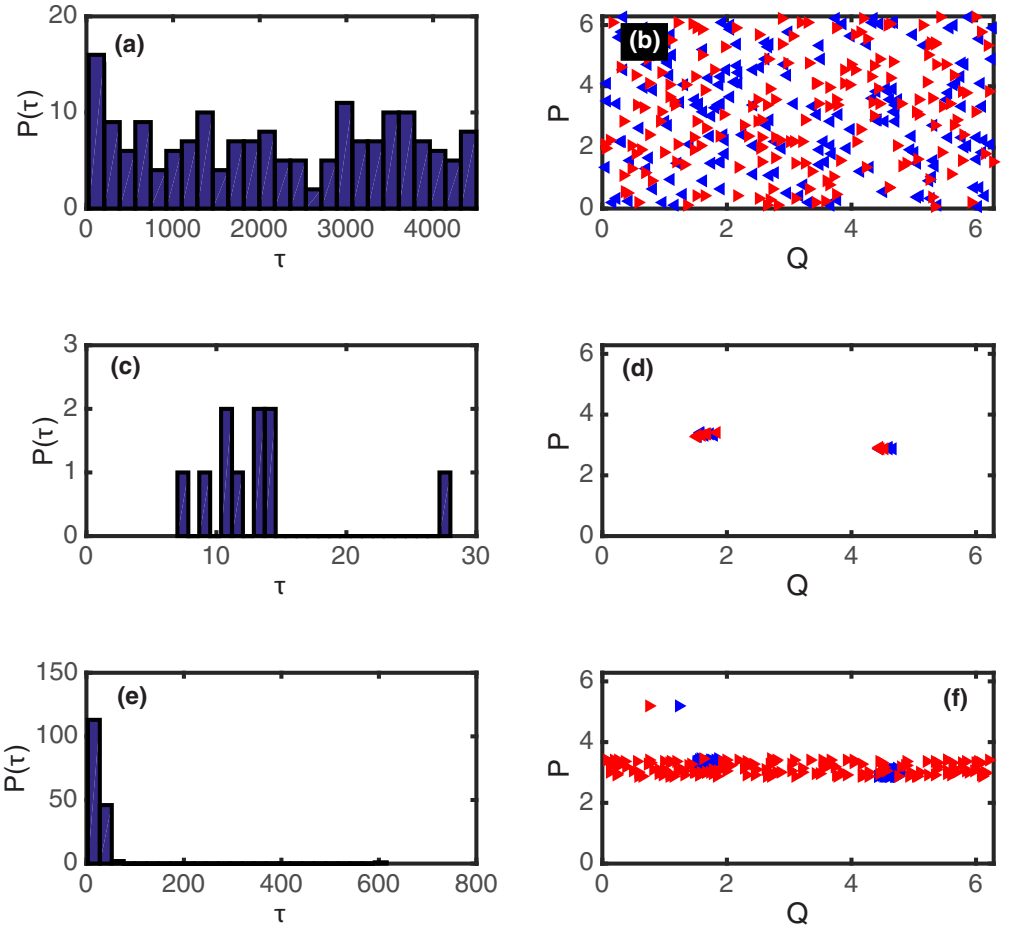

FIG. 10. The distribution of synchronization times and location of initial conditions for the coupled standard map at $K = 6.0$ for (drive, response) maps in the [(a) and (b)] (chaotic, chaotic) regime, [(c) and (d)] (regular, regular) regime, and [(e) and (f)] (regular, chaotic) regime. The initial conditions for the drive map are plotted using the left hollow triangle, "◁" in blue, and for the response map using the right hollow triangle, "▷" in red, in the plots. Complete synchronization is taken to be achieved if the iterates fall within a distance 10^{-5}. For more details, see the text in Sec. III. The histograms on the left show synchronization times from 50 000 initial conditions randomly chosen from the uniform distribution on the interval $[0,2\pi]$. The data are binned into 25 bins. The locations of initial conditions in the plots on the right of the panel indicate the regions from which these initial conditions are chosen (here, only 500 initial conditions are plotted). It may be noted that we did not find any (chaotic, regular) pair that synchronizes.

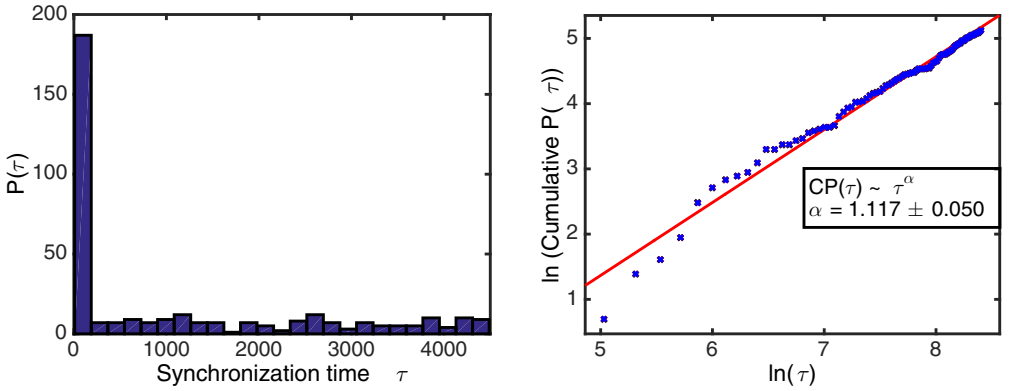

FIG. 11. The distribution of synchronization times for the coupled standard map at $K = 6.0$. (a) The distribution of synchronization times for evolution from 50 000 initial conditions randomly chosen from the uniform distribution on the interval [0,1]. The data are binned into 25 bins. (b) The long tail in the distribution shows power-law behavior as seen in the log-log plot of the cumulative distribution. The exponent α for the fit shown takes the value 1.117 ± 0.050.

area-preserving standard map using the method of parameter perturbation [29]. The perturbation is applied in the local neighborhood of the periodic points of the map. The area-preserving nature of the map is to be kept intact. We describe the method briefly.

We take the following form of the standard map:

$$\left.\begin{aligned} P_{n+1} &= P_n + \tfrac{K}{2\pi}\sin(2\pi Q_n) \\ Q_{n+1} &= P_{n+1} + Q_n \end{aligned}\right\} \bmod 1. \qquad (17)$$

Here $-0.5 \leqslant P_n \leqslant 0.5, 0 \leqslant Q_n \leqslant 1$, where n denotes the discrete time, and K is the nonlinearity parameter as seen previously. In the form above [30], the standard map is known to have a hyperbolic fixed point at (0,0.5). We perturb the parameter K to $K - \epsilon$ if $|P - P_f| < \delta, |Q - Q_f| < \delta$. For P and Q outside this δ strip, K does not change. It may be noted that the Jacobian J of the original standard map is given by

$$J = \begin{bmatrix} 1 & 1 + K\cos(2\pi Q_n) \\ 1 & K\cos(2\pi Q_n) \end{bmatrix}.$$

The determinant of this matrix is 1 as the dynamics is area preserving. This remains at unity for the perturbed map also in which K is replaced by $K - \epsilon$ [31]. The coherent structure thus obtained for $K = 6$, $\delta = 0.3$, and $\epsilon = 2$ about the fixed point $(P_f, Q_f) = (0.0, 0.5)$ is shown in Fig. 12(a).

We now examine the synchronization of the perturbed maps above, when the maps are coupled using the Pecora-Carroll method. With the introduction of a coherent structure in the coupled system at $K = 6$ with the perturbation parameters as above, the response map also develops an identical structure in the phase space [see Fig. 12(b)] due to synchronization. Here the perturbation is applied to both the drive and the response maps. We find that synchronization times reduce remarkably after the introduction of the coherent structure. This indicates that the parameter perturbation forces the trajectories of the drive and response maps to stick around the coherent structure and therefore leads to considerably shorter synchronization times. In addition to this, we observe that the percentage of initial conditions which show synchronization increases to about 7%, which is an increase by a factor of 10 as compared with the fraction of initial conditions which synchronize seen in the case of the unperturbed map. Thus, the basin of synchronization is greatly enhanced. In quantitative terms, we find that the distribution of synchronization times is now exponential as shown in Fig. 13 with the exponent $\mu = 326.45 \pm 10.89$ for 50 000 different initial conditions randomly chosen from the uniform distribution on the interval [0,1]. Therefore, the heavily long-tailed distribution seen in the unperturbed map (Fig. 11) turns into an exponential distribution in the presence of the coherent structure induced by the perturbation (Fig. 13).

If the phase space of the unperturbed map is predominantly chaotic (as at $K = 6$), the creation of a coherent structure leads to a much larger enhancement in the fraction of synchronizing initial conditions (a factor of 10 at $K = 6.0$) than for the case where the mixed phase space has more regular regions in the

TABLE II. The tail of the distribution of synchronization times shows power-law behavior for the cases reported here. The table gives the value of the exponent for various classes of initial conditions for all possible pairs at $K = 1.5, 4.0$, and 6.0 for 5000 and 10 000 iterations as indicated. The exponents have been estimated from the log-log plot of the corresponding cumulative probability distribution. A pair (C,R) indicates the (Chaotic, Regular) class, etc. It is to be noted that no synchronizing (C,R) pair was found at $K = 6.0$.

	(Chaotic, Chaotic)		(Chaotic, Regular)		All	
K	5000	10 000	5000	10 000	5000	10 000
1.5	1.022 ± 0.044	0.820 ± 0.032	0.974 ± 0.035	0.792 ± 0.028	0.917 ± 0.030	0.729 ± 0.024
4.0	1.105 ± 0.045	1.055 ± 0.021	1.156 ± 0.045	1.039 ± 0.016	1.081 ± 0.030	1.031 ± 0.021
6.0	1.120 ± 0.033	1.175 ± 0.022			1.117 ± 0.034	1.175 ± 0.023

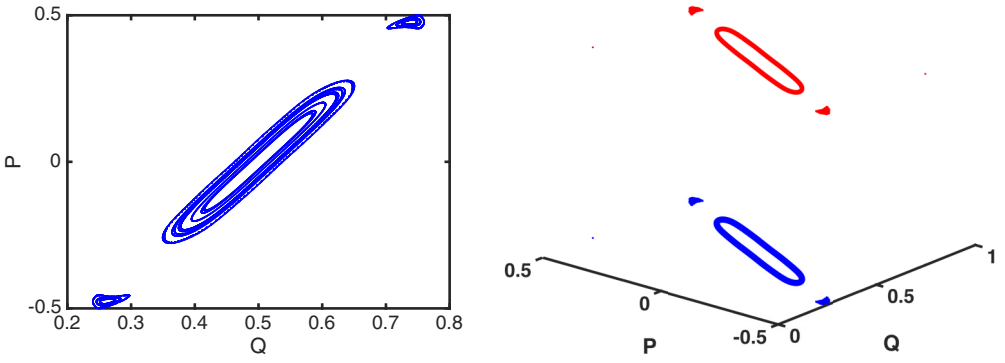

(a) (b)

FIG. 12. (a) The coherent structure in the phase space of the standard map for $K = 6.0$, $\delta = 0.3$, and $\epsilon = 2.0$ about the fixed point $(P_f, Q_f) = (0.0, 0.5)$. (b) Synchronization is seen in the phase space of the drive and response maps in the presence of the coherent structure. This plot is for $K = 6.0$ and for perturbation values as given in the text. We evolve 25 initial conditions chosen randomly from the uniform distribution on the interval [0,1] for 4500 iterations. The transient is 500 iterates.

first place, as at $K = 1.5$, where regular regions occupy about half of the phase space. Here the creation of coherent structures enhances the number of synchronizing initial conditions by only about 20%. The size of the newly created structure also has a role to play in this enhancement, as larger coherent structures lead to shorter synchronization times.

VI. CONCLUSIONS

To summarize, we have explored different aspects of the phase synchronization observed in area-preserving maps, coupled by the Pecora-Caroll method. Coupled standard maps show complete phase synchronization, with intermittent behavior in the presynchronized transient for the phase difference for initial conditions that are uniformly distributed. This intermittency shows power-law behavior. We have also shown that synchronization occurs when the drive and response trajectories are in the sticky regions close to the invariant curves in the phase space. Stable periodic trajectories exist in these neighborhoods and the existence of local transverse stable directions encourages trajectories to synchronize, leading to laminar regions in the time series of the separation between trajectories, interspersed by chaotic bursts which are seen when the trajectories leave these neighborhoods. This is similar but opposite to the effect seen due to unstable periodic trajectories in the studies of Heagy, Pecora, and Carroll [22].

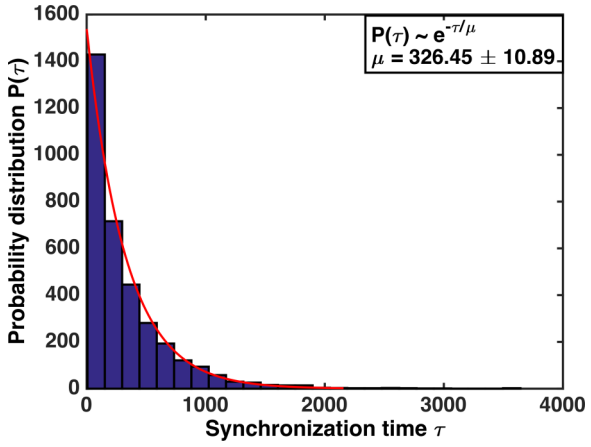

FIG. 13. The probability distribution for the distribution of synchronization times of the coupled standard map system with a coherent structure created via perturbation shows exponential behavior as shown in the figure. The perturbation is applied in the neighborhood of the fixed point $(P_f, Q_f) = (0.0, 0.5)$ with $K = 6.0$, $\delta = 0.3$, and $\epsilon = 2.0$. The distribution of synchronization times is obtained for for 50 000 different initial conditions randomly chosen from the uniform distribution on the interval [0,1], divided into 25 bins. The exponent of the distribution is found to be $\mu = 326.45 \pm 10.89$. The mean synchronization time for this case is 326.44.

The distribution of synchronized times depends crucially both on the parameter value of the nonlinearity parameter K as well as on the mixed nature of the phase space. Distributions of synchronized times show long-tailed behavior with accompanying power laws for initial conditions distributed uniformly in the phase space, as well as for some combinations of drive and response initial conditions in the regular and chaotic regimes. The introduction of a coherent structure in the system drastically alters the distribution of synchronization times, which crosses over to exponential behavior, and also drastically enhances the size of the basin of synchronization. Thus, the introduction of a coherent structure can be an effective strategy in cases where short synchronization times are desirable.

We note that most of the novel aspects of synchronization seen here come from the existence of a mixed phase space and the consequent sensitivity to initial conditions. We note that many of these effects are similar to those seen in the case of coupled dissipative systems due to the presence of riddled basins of attraction and attractor bubbling bifurcations [12,32,33]. The precise correspondence between these aspects, and the phenomena seen here due to the mixed nature of the phase space, needs to be explored further. Additionally, phenomena such as the phase slips seen in coupled rotating Rayleigh-Benárd convection systems are also a consequence of the mixed nature of the phase space and the effects of local stable and unstable directions. Despite the genericity of the standard map, we have not observed phase slip effects

in our studies of the standard map. These effects, however, are easily observed in other area-preserving maps such as the Blinking Vortex map of Aref [34]. We plan to study these effects elsewhere.

ACKNOWLEDGMENT

One of us (N.G.) thanks CSIR (India) for partial financial support via the Grant 03(1294)/13/EMR-II.

[1] J. Klafter and G. Zumofen, Phys. Rev. E **49**, 4873 (1994).
[2] G. M. Zaslavsky, Phys. Rep. **371**, 461 (2002).
[3] G. M. Zaslavsky, Physica D **168-169**, 292 (2002).
[4] L. M. Pecora and T. L. Carroll, Phys. Rev. Lett. **64**, 821 (1990).
[5] L. M. Pecora and T. L. Carroll, Phys. Rev. A **44**, 2374 (1991).
[6] R. Roy and K. S. Thornburg, Phys. Rev. Lett. **72**, 2009 (1994).
[7] N. F. Rulkov, M. M. Sushchik, L. S. Tsimring, and H. D. I. Abarbanel, Phys. Rev. E **51**, 980 (1995).
[8] L. Kocarev and U. Parlitz, Phys. Rev. Lett. **76**, 1816 (1996).
[9] R. Brown and N. F. Rulkov, Chaos **7**, 395 (1997).
[10] H. Ulrichs, A. Mann, and U. Parlitz, Chaos **19**, 043120 (2009).
[11] L. M. Lopes, S. Fernandes, and C. Grácio, Nonlinear Dyn. **79**, 1615 (2015).
[12] L. M. Pecora and T. L. Carroll, Chaos **25**, 097611 (2015).
[13] J. F. Heagy and T. L. Carroll, Chaos **4**, 385 (1994).
[14] A. Hampton and D. H. Zanette, Phys. Rev. Lett. **83**, 2179 (1999).
[15] X. W. Wang, M. Zhan, C.-H. Lai, and H. Gang, Phys. Rev. E **67**, 066215 (2003).
[16] U. E. Vincent, New J. Phys. **7**, 209 (2005).
[17] L. M. Pecora, T. L. Carroll, G. A. Johnson, D. J. Mar, and J. F. Heagy, Chaos **7**, 520 (1997).
[18] S. Boccaletti, J. Kurths, G. Osipov, D. L. Valladares, and C. S. Zhou, Phys. Rep. **366**, 1 (2002).
[19] A. Pikovsky, M. Rosenblum, and J. Kurths, *Cambridge Nonlinear Science Series 12* (Cambridge University Press, Cambridge, 2001).
[20] B. V. Chirikov, Phys. Rep. **52**, 263 (1979).
[21] J. D. Meiss, Chaos **25**, 097602 (2015).
[22] J. F. Heagy, T. L. Carroll, and L. M. Pecora, Phys. Rev. E **52**, R1253 (1995).
[23] L. M. Pecora and T. L. Carroll, Phys. Rev. Lett. **80**, 2109 (1998).
[24] W. K. Wong, B. Zhen, J. Xu, and Z. J. Wang, Chaos **22**, 033146 (2012).
[25] G. M. Zaslavsky, M. Edelman, and B. A. Niyazov, Chaos **7**, 159 (1997).
[26] G. M. Zaslavsky and B. A. Niyazov, Phys. Rep. **283**, 73 (1997).
[27] J. D. Szezech, Jr., S. R. Lopes, and R. L. Viana, Phys. Lett. A **335**, 394 (2005).
[28] T. S. Parker and L. O. Chua, *Practical Numerical Algorithms for Chaotic Systems* (Springer-Verlag, New York, 1989).
[29] N. Gupte and A. Sharma, Phys. Lett. A **365**, 295 (2007).
[30] The range of P and Q has been chosen such that the coherent structure appears at the center of the phase space plot.
[31] A. Sharma and N. Gupte, Pramana J. Phys. **48**, 231 (1997).
[32] J. F. Heagy, T. L. Carroll, and L. M. Pecora, Phys. Rev. Lett. **73**, 3528 (1994)
[33] S. Yanchuk, Y. Maistrenko, and E. Mosekilde, Physica D **154**, 26 (2001).
[34] H. Aref, J. Fluid Mech. **143**, 1 (1984).